

Pushing the envelope: HI-CLASS Range and Range-rate

Dr. Paul Konkola¹, Charles Crandall, Tim Georges, Robert Lercari (Textron Systems)
Moe Tun (Advanced Technology Corp)
Laura Ulibarri, Jill Watson (Air Force Research Laboratory)

Abstract

The HI-CLASS (High Performance CO₂ LAdar Surveillance Sensor) operating in conjunction with the AEOS 3.6 meter aperture telescope atop Mt. Haleakala has demonstrated its ability to produce simultaneous precision range (4m in narrow band; 10 cm in wide band), range rate, and angular position measurements (FWHM beam width of 4 micro-radians) of both uncooperative ($> 0.1 - 0.2$ m diameter) in LEO trajectories and cooperative (retro) satellites. We describe key improvements and investigations into the system that are helping to extend the system's range accuracy toward its precision. The limiting range-rate error source is also addressed. Specifically, the impacts of the timing system, the electronic time delays, and the local oscillator stability on the metric accuracy are assessed.

1. Introduction

HI-CLASS² is a coherent laser radar system providing precision range and range-rate measurements and range-Doppler imaging. It was designed for tracking and imaging of space objects. Also, its imaging functionality makes it well suited for missile defense applications. The system has a nominal design sensitivity for detecting satellites with reflectivity area products of 1 m^2 at 10 Mm. The system can output 12 J per pulse at 15 Hz. The transmitter, which is shown in Figure 1, is based on a transverse excited atmospheric (TEA) CO₂ laser operating at 11.15 microns. The 11.15 micron wavelength has a 92% transmission efficiency³ from Haleakala (10,000 ft elevation) looking straight up. This wavelength also has a high turbulence efficiency where r_0 looking straight up is approximately 6 – 8 m. Therefore, it is well suited for large aperture projection such as through the 3.6 m AEOS telescope shown in Figure 2. The laser is eye safe out of the telescope.

The original design precision of 4 m in range has been exceeded by demonstrations of 0.1 m in its pulse-burst format. While the laser waveform is expected to allow sub-10 cm precision, the accuracy is currently limited by other sources of error.

The HI-CLASS ranging data is compared to orbits derived from International Laser Ranging Service data for the Lageos satellite. The resulting residual is a measure of the

¹ konkola@alum.mit.edu, 535 Lipoa Pkwy, Suite #149, Kihei, HI 96753

² M. Groden, D. Brown, R. Eng, M. Kovacs, P. Lewis, R. Pohle, K. Ayers, J. Gonglewski, S. Czyzak, D. Werling, L. Crawford, "HI-CLASS on AEOS: A Large Aperture Laser Radar for Space Surveillance / Situational Awareness Investigations", Proceedings of the 2001 Space Control Conference (April 2001).

³ From Plexus Release 3.0 Version 2.0, 23 Km visibility assumed.

HI-CLASS accuracy down to the sub 10 cm uncertainty level. This paper investigates errors associated with the timing system and electronic time delays in the receiver in an effort to improve the absolute accuracy of the system. The measurement method and results for the time base and jitter errors is presented. Frequency dependent time delays arise since HI-CLASS is a heterodyne system and delay through the receiver varies depending on the frequency of the beat note. As a result, filter calibrations are required to compensate for the non-constant time delay inherent in the electronic channels of the outgoing pulse monitor (OPM) and the received signals. These signals have a varying frequency on a pulse-to-pulse basis that is largely dependent on the local oscillator-to-seed locking stability and the Doppler shift from the target that is un-cancelled electronically. The method and procedure for calibrating the time delays is presented.

The range-rate precision and accuracy has been assessed to be limited by the stability of the local oscillator during the time of flight. This assessment is supported by cm/s level noise floor measurements at short range. Also the stability of the local oscillator when referenced against an ultra-stable laser is consistent with the velocity noise floor measured against space objects when considering the time of flight. Data is presented for velocity measurements that are corrected using the beat signal between an ultra-stable laser and the local oscillator.



Figure 1 The TEA laser is the large chamber indicated. The bench in front of it holds transmitter optics and the seed laser.



Figure 2 The 3.6 m AEOS telescope on top of Mt Haleakala where a HI-CLASS transmitter and receiver is installed.

HICLASS employs two waveforms shown in Figure 3. The top plot shows the heterodyne pulse tone waveform. The pulse body is on the order of 4-6 microseconds typically. There is a gain switched spike with a FWHM of approximately 200 ns. The narrow gain switched spike enhances the range resolution while the wide pulse body is desirable for fine velocity resolution. The uncertainty in the range for acquisition of an object for the pulse tone format can be 18 Km without undergoing any search for the object. The pulse tone range sigma has been demonstrated to be 4 m for high signal to noise signals from satellites. In-lab data has shown range standard deviation of about 2 meters for high SNR data. The lower plot shows the mode locked pulse-burst waveform. The micropulses are separated by 40 ns. The width of the individual micropulses can be 1.5 ns, contributing to its higher range precision over the pulse tone format. Range precision of 0.1 m has been demonstrated⁴. The pulse-burst format enables the system to function as an imaging lidar. The acquisition window is 5 km in the pulse burst format, which favors the pulse tone for acquisition. The pulse tone format has a simpler signal processing requirement and it has been used extensively for real-time metrics. While the system can toggle between pulse tone and pulse burst on a shot-to-shot basis, only the accuracy of the pulse tone format is the subject of this paper.

⁴ D. Currie, P. Konkola, M. Kovacs, R. Pohle, "HI-CLASS Ranging Accuracy Assessment Using Geodyn", Proceedings of the 2005 AMOS Technical Conference (September, 2005).

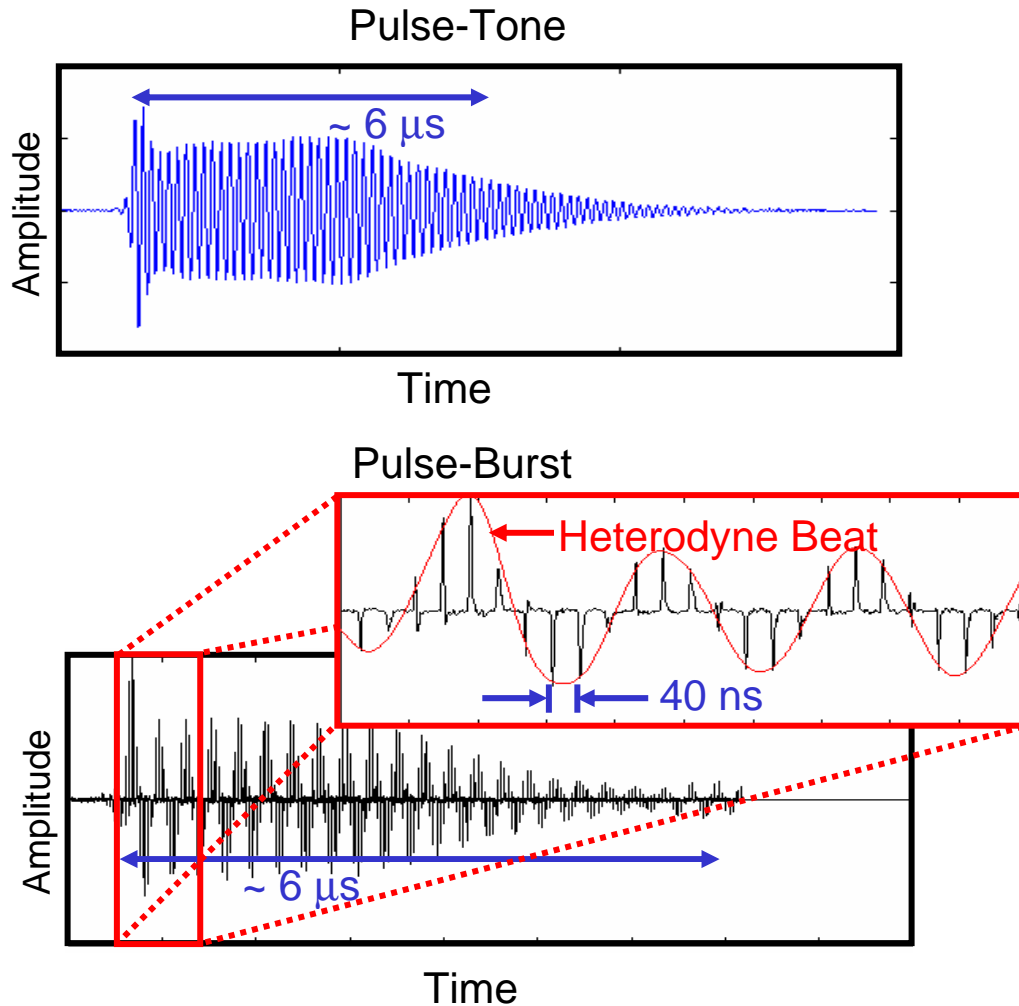


Figure 3 The top plot shows the pulse tone heterodyne waveform. The lower plot is the pulse burst waveform. It is a mode locked pulse tone waveform with 40 ns micropulse spacing.

A simplified diagram of the hardware configuration for HI-CLASS is shown in Figure 4. The laser transmitter achieves single mode operation by cavity matching to a seed laser. The seed laser is locked to the local oscillator by use of a seed locking controller and detector. The beat frequency between the seed and local oscillator is nominally set to 6 MHz. The system uses a holey mirror as a transmit and receive switch. Since the telescope moves during the time-of-flight, the return beam deviates in angle from the receive beam. The angle between the transmit and receive beam is given by $\alpha = 2 v_{\theta}/c$. Here v_{θ} is the cross-range velocity of the object and c is the speed of light. The telescope points ahead while tracking the object and the track lag mirror keeps the return signals stationary on the receiver detector and acquisition cameras. The received beam is beat with a local oscillator that may be acousto-optically shifted to ensure the return signal is always greater than 500 MHz. The receiver tracks out the Doppler shift and brings the signal down to base band for in-phase (I) and quadrature (Q) signals, which are separated by a phase shift of 90 degrees. Finally, a data acquisition system digitizes and records the OPM, I, and Q signals.

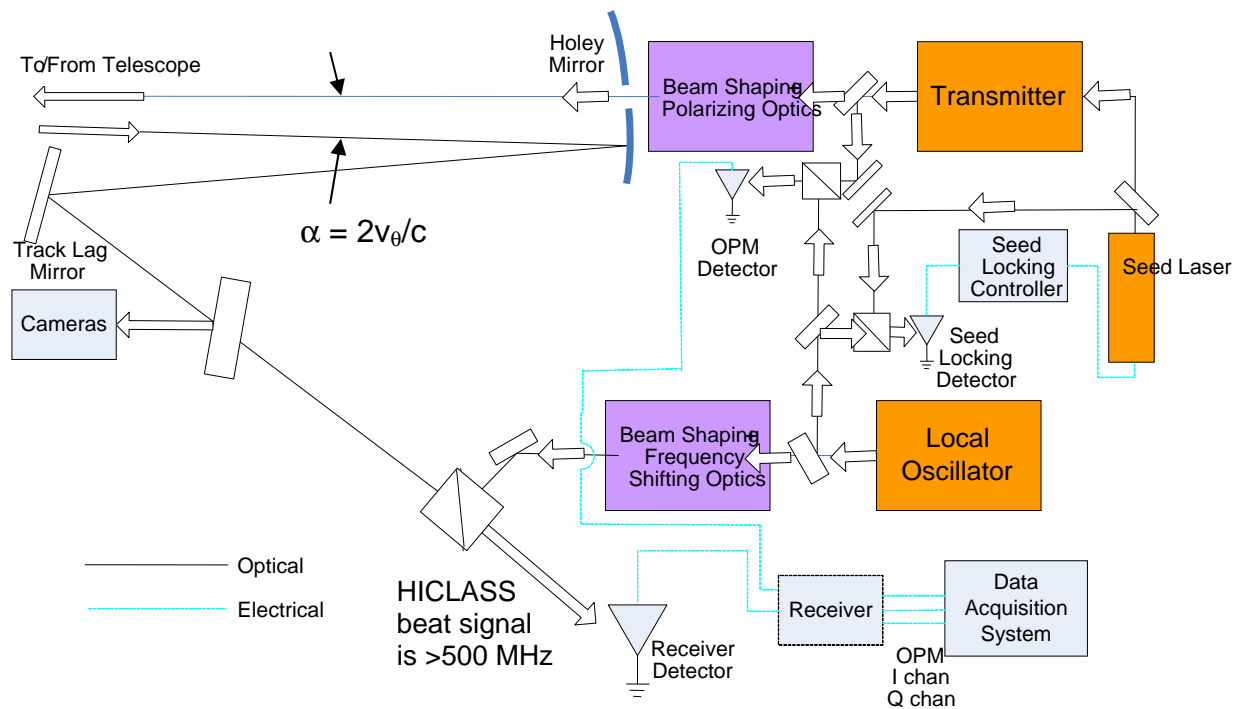


Figure 4 A simplified diagram of the HI-CLASS heterodyne laser radar.

2. Ranging accuracy assessment method

Highly accurate ephemeris can be calculated using International Laser Ranging Service (ILRS) data and sophisticated orbit determination techniques. Calculated ephemeris of the Lageos satellites can have centimeter level accuracy⁵. We employ the Orbit Determination Tool Kit from AGI and ILRS data from the Lageos satellites to obtain the highly accurate orbital reference data. The expected accuracy of our calculated ephemeris was assessed using a previously used validation approach⁴. Figure 5 shows normal point residuals of the ILRS tracking stations for a Lageos-I pass on Sept 29, 2003. This plot shows the centimeter-level residuals that are typical of ILRS normal point data. To assess the orbit determination accuracy for a HI-CLASS-like scenario, the Haleakala tracking station known as LURE was not used in the “truth orbit” calculation. Instead, its residual from an orbit calculated using all the other ILRS stations is shown. In this way, possible questions of the orbital accuracy for a remote location, far from other ILRS stations, are eliminated. ILRS data from Sept 22-Oct 4, 2003 was used to determine the orbit. The shown sub-8 cm accuracy is the expected level of accuracy for ephemeris using our current approach. Since this accuracy was considered excellent for this phase of the work, potential refinements in the orbit determination process were not pursued. While LURE is no longer operational, its archived data corroborates the ILRS-based technique since the same level of ephemeris accuracy is expected for HICLASS comparisons.

⁵ R. Noomen, “Precise Orbit Determination with SLR: Setting the Standard”, *Surveys in Geophysics* 22: 473-480, 2001.

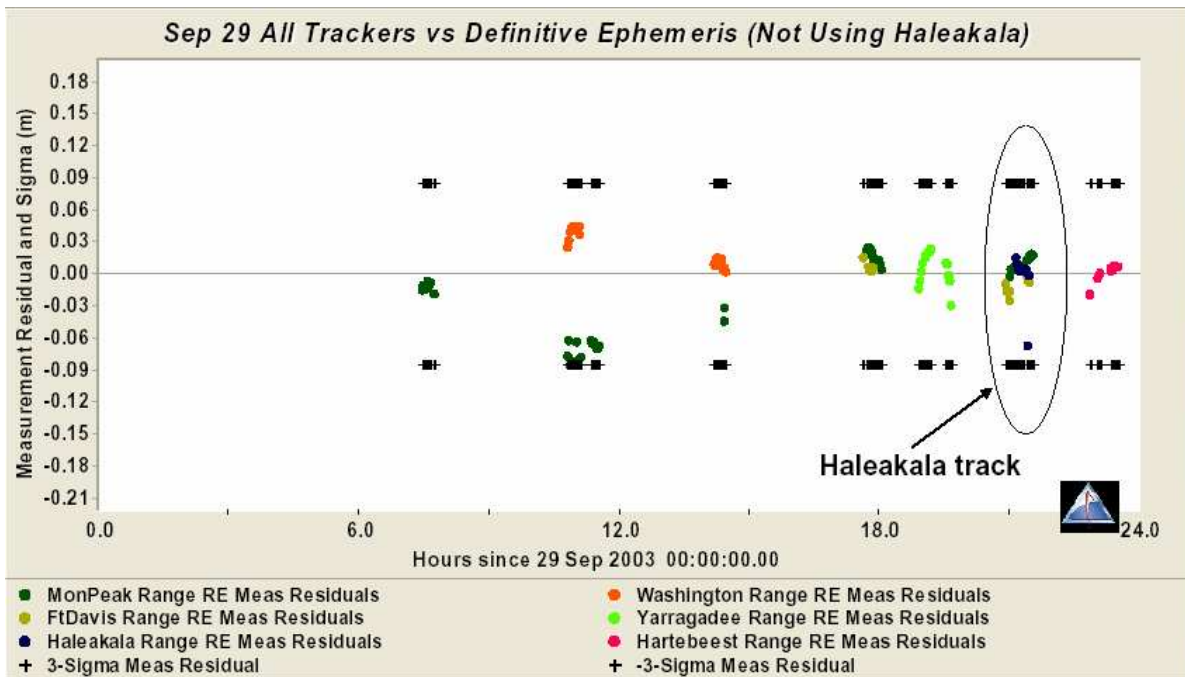


Figure 5 Range residuals of ILRS tracking stations for the Lageos-I satellite on September 29. All stations shown but Haleakala were used to generate the orbit. Residuals of all tracking stations, including Haleakala, to this orbit are shown.

Figure 6 shows the HI-CLASS residuals from seven Lageos II passes that occurred on April 25 to May 3, 2005. The standard deviations ranged from 3.5 to 4 meters, which is typical and not a concern for the pulse tone format. The average bias in the plot would be subtracted for real-time data. Most importantly, the mean residual from each pass varied by ± 2 m. This is a statistically significant instability considering that each pass had many hundreds to several thousand data points.

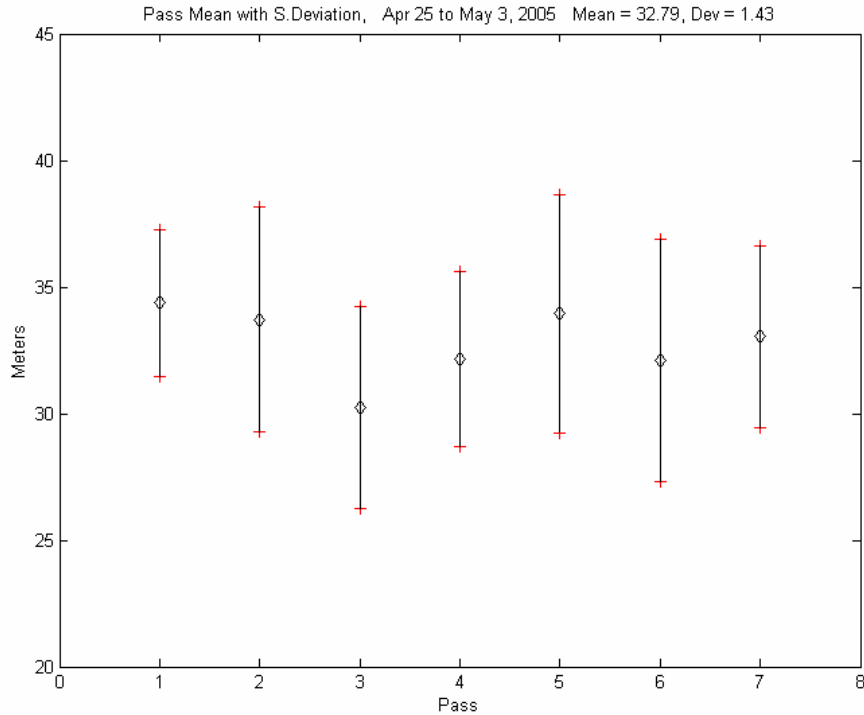


Figure 6 HI-CLASS residuals for seven Lageos II passes on April 25 to May 3, 2005.

Two issues were identified after observing the pass to pass bias instability. The system timing stability and time delays are the subjects of the next two sections.

3. Timing System Accuracy

The system timing accuracy was assessed using the setup in Figure 7. The timing of the HI-CLASS system is based on a delay generator that triggers the data acquisition on OPM and two receive A/D boards. The delay between triggering the OPM and received boards is programmed into the delay generator on a shot-to-shot basis and its value is based on an estimate of the time-of-flight of the laser pulse. For instance element sets can be used to provide a range estimate with typical accuracies of 5 km. For in-lab testing, the OPM to receiver A/D delay is user controllable. The timing test was conducted to measure the timing errors over the operational times of flight (up to 67 ms) by adjusting the user controllable range delay. The input to the A/D cards was a CMOS square wave from a recently calibrated CG635⁶ with the rubidium time base option. Its maximum error over a whole year is specified as less than 0.5 ppb.

⁶ From Stanford Research Systems, Sunnyvale, CA, www.thinksrs.com.

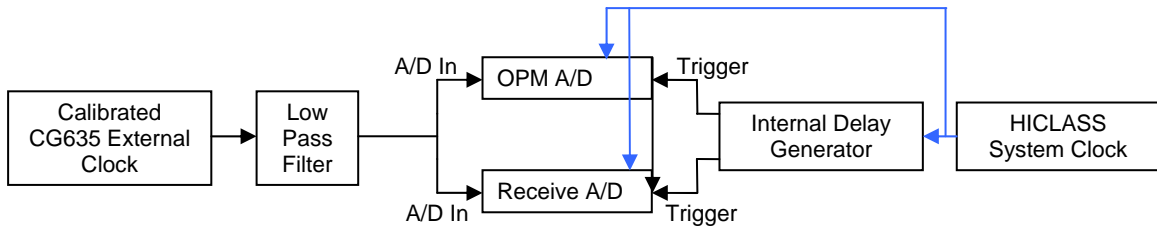


Figure 7 The timing test setup.

The principle of the timing test can be seen from Figure 8. The clock period, T_{clock} , must be known accurately for the integer number of clock periods to be known very accurately. For a perfect instrument

$$N * T_{clock} = T_{delay} + T_{rec} - T_{opm} \quad (1)$$

Where N is an integer number of clock periods and T_{delay} is the delay programmed into delay generator. The variables T_{rec} and T_{opm} are found experimentally and are defined as the time to the first rising edge in the data acquisition windows. In a real system, Equation 1 is never exactly satisfied and the timing error is given by the difference between left and right hand sides of the equation, such that

$$Timing_error = round[(T_{delay} + T_{rec} - T_{opm}) / T_{clock}] * T_{clock} - (T_{delay} + T_{rec} - T_{opm}). \quad (2)$$

The system time-base error and jitter is assessed from the mean and standard deviation of the $Timing_error$ respectively.

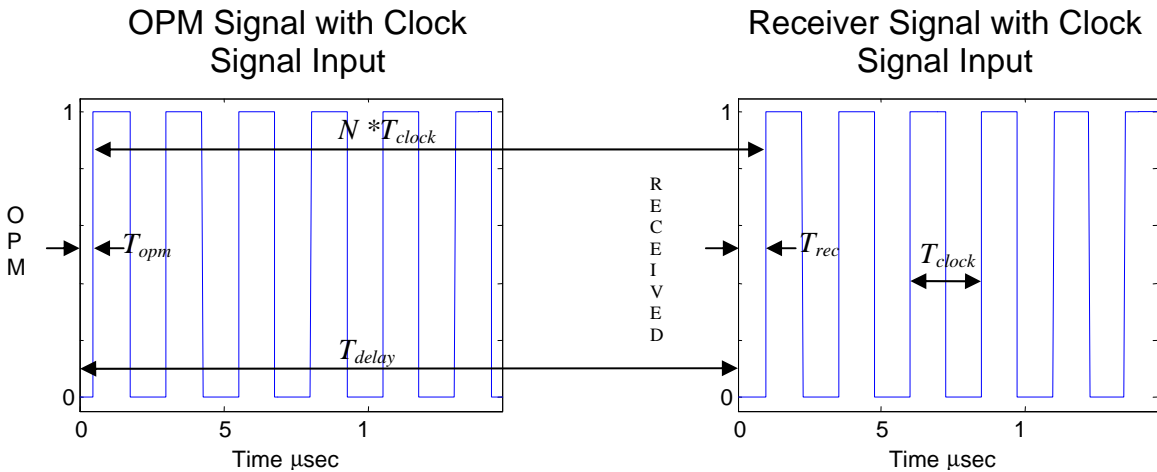


Figure 8 Timing test concept. Since the time between rising edges is known very accurately, the HICLASS system timing error can be assessed.

Through this test, we confirmed the timing accuracy using a calibrated reference. We concluded that the old clock had a time base error of 0.65 ppm. Furthermore, an investigation into the range calculation revealed that the old system used a rounded value of the speed of light contributing another 0.14 ppm of error. Both errors contributed to an inaccurate reported range such that

$$Reported_range = (1 - 0.79e-6) * real_range. \quad (3)$$

This time base is consistent with the ranging data shown in Figure 6 and again plotted in Figure 9. In this figure the residual is plotted versus range. The expected slope of 0.79 ppm is corroborated by the experimentally determined slope of 0.84 with uncertainty in the linear regression of 0.07 ppm. Considering that the HI-CLASS system is designed for ranging on satellites out to 10 Mm, the time-base error could contribute almost 8 m of error.

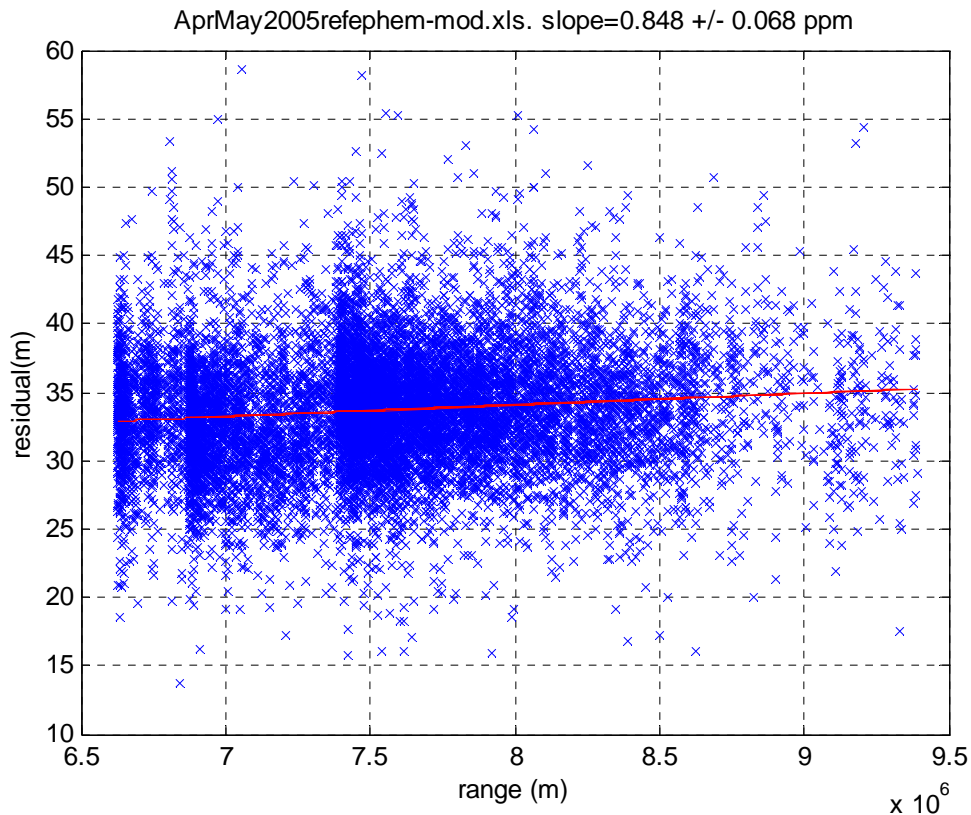


Figure 9 Residuals of HI-CLASS from seven Lageos-II passes plotted versus range. The time base error is evident by the slope.

The old time base was not expected to drift very fast and may have been largely calibratable. However, since even 10 cm level errors were of interest, the time-base was upgraded. The system time base now is the Stanford Research Systems CG635 with the rubidium time base option. The effective time-base error of the HI-CLASS system was verified against a second calibrated external clock to be *accurate* to better than 1 ppb in pulse tone and pulse burst. This expected result thoroughly confirms the time base accuracy of the data acquisition system. The system timing jitter also demonstrated excellent performance. In pulse tone, the timing jitter was measured to be 0.3 ns, which corresponds to a standard deviation in range of 5 cm. A low pass filter was used on the external CG635 to obtain a 38 nsec rise time (10%-90%) reference. The timing is a result of interpolating the 70 MHz A/D sampled signal. Even though the pulse burst signal is sampled at 1 GHz, the measured timing jitter of 0.5 ns sigma in this mode was actually worse than the slower sampled pulse tone data. The pulse burst timing was measured

using a 3.5 nsec (10%-90%) rise time reference. Nevertheless, both the pulse tone and pulse burst modes demonstrate excellent timing system performance.

While the clock upgrade resulted in a significant performance improvement and the timing system characterization allows the timing system to be ruled out as a significant source of error, other significant errors in the system remain. The next section investigates the significant errors associated with the time delays in the receiver.

4. Electronic Time Delays

A heterodyne receiver is used to amplify the OPM and receive detector signals, provide low pass filtering for anti-aliasing, track out the Doppler shift of the return signal, and provide in-phase and quadrature signals for the received signal. Figure 10 shows the block diagram of the heterodyne receiver. The delay through the receiver is dependent on the frequency of the OPM and received signals. The OPM has a varying frequency based on the LO-to-Seed frequency locking stability. The receiver delays are also dependent on the target Doppler-to-receiver tracking. While the receiver dependent delays will be different on a shot-to-shot basis, range corrections can be performed based on the OPM and receiver frequency-dependent time delays

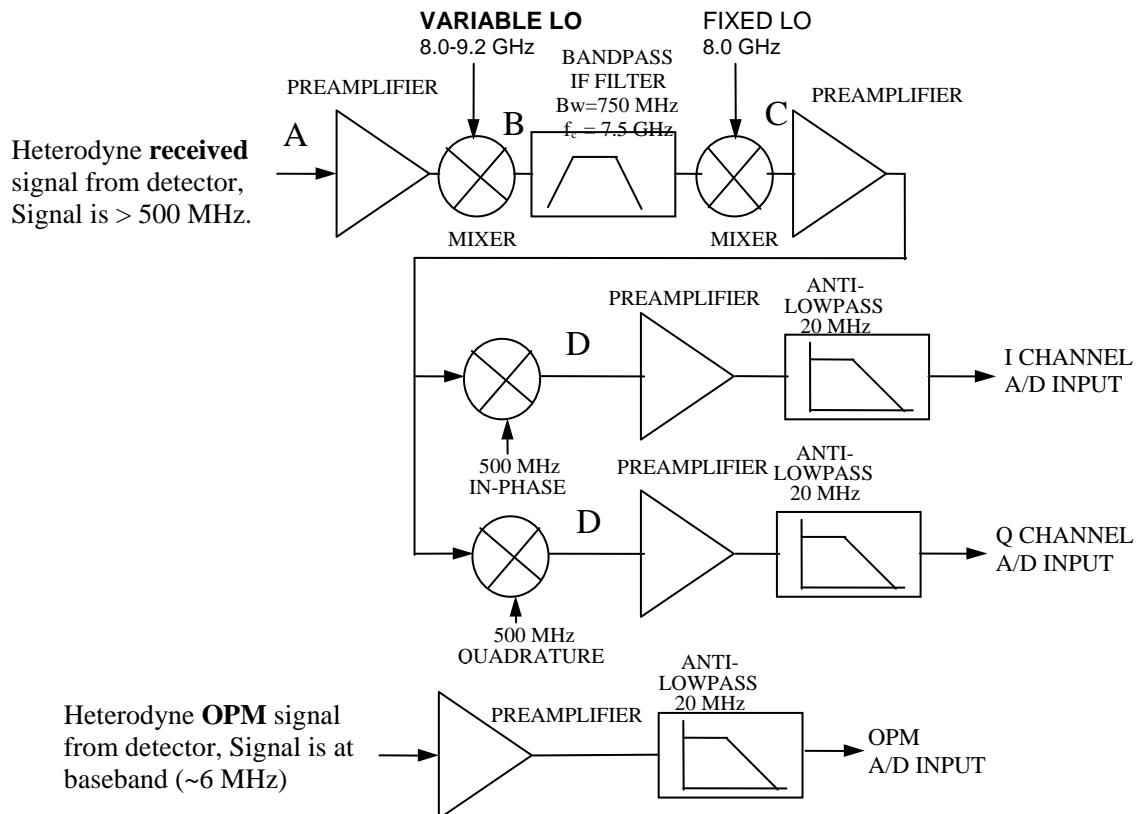


Figure 10 Heterodyne Receiver Block diagram for the pulse tone signals

The OPM chain is relatively simple. The OPM is preamplified and then followed by an anti-alias filter with approximately 20 MHz bandwidth. The receiver chain is more complicated as it is designed to track out the Doppler shift of the target. Furthermore, the receiver is designed such that it requires a frequency greater than 500 MHz at point “A” to function correctly.

A satellite has a larger Doppler shift when it is low in the horizon. As the satellite rises, the range-rate decreases. When its range rate decreases below 2.79 km/s ($500\text{MHz} \cdot 11.15 \mu\text{m}/2$), an acousto-optically shifted local oscillator beam contributes an additional 500 MHz of optical shift. Since at culmination the Doppler shift from the target is zero, the local oscillator needs to be able to produce optical frequency shifts of 500 MHz. Past culmination, a *negative* 500 MHz shifted beam beats with the received beam. As the object falls, the Doppler shift increases and the unshifted local oscillator is selected when the Doppler shift from the target exceeds 500 MHz again. The requirement for a greater than 500 MHz optical difference between the local oscillator and receive beams arises from the wide band width of the optical signal in pulse burst mode. The mode-locked laser spectra has positive and negative sidebands as illustrated in Figure 11. The center frequency is at the seed frequency plus the Doppler shift from the target. The frequency spread typically has significant energy out to ± 200 MHz or more. Since the optical signal is greater than 500 MHz, the positive and negative sidebands do not wrap around base band. The large offset from DC also places the signal far away from the low frequency $1/f$ noise of the detector.

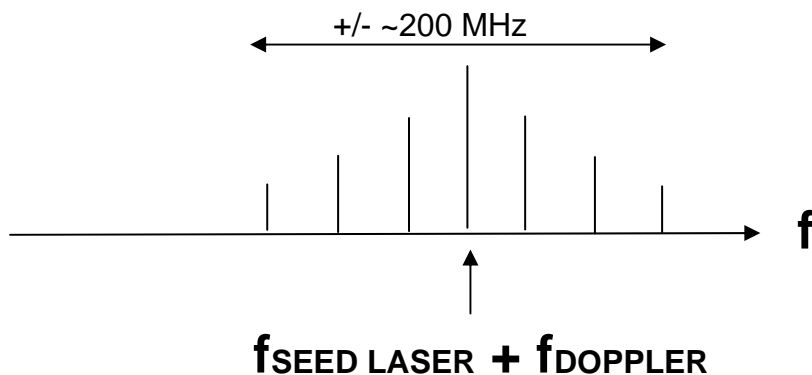


Figure 11 Frequency spectra of a mode locked laser showing that there are positive and negative sidebands about the nominal.

At point B the signal has been beat with a variable frequency oscillator to stabilize the frequency of the signal through the rest of the circuit. The programmed VFO frequency is based on an estimate of the target Doppler. Since the estimate is imperfect, the received signal has an associated variability in frequency. At this point in the circuit, the signal is centered at 7.5 GHz and is filtered with a ± 375 MHz bandpass filter. A fixed 8.0 GHz mixer beats the signal down to 500 MHz at point C. The final pair of mixers, which are at 500 MHz but off by 90 degrees, produces in-phase (I) and quadrature (Q) signals that are also 90 degrees apart. The I and Q channels allow for DC level signals even though they wrap the positive and negative frequencies about 0 Hz. The anti-alias low pass filter is at 20 MHz for pulse tone and at about 400 MHz for pulse burst.

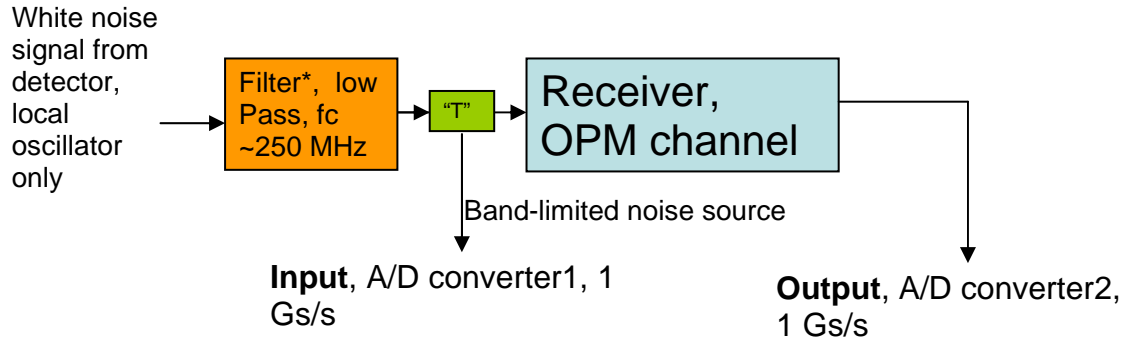


Figure 12 Frequency response test setup for the OPM channel.

The frequency response for the OPM is obtained using the setup in Figure 12. Here a white noise signal is applied to the OPM channel and the frequency response is derived from $\text{FFT}(\text{Output})/\text{FFT}(\text{Input})$. A high resolution frequency response for the OPM channel is shown Figure 13.

The FFT length was 16384 data points. Sixteen sets of one million samples each were averaged using an overlap of half the fft length resulting in 1936 averaged data sets. The resulting frequency response has a sufficiently fine resolution of 61 KHz with very little noise.

Additional tests confirmed that the distortion of the fast sampling (1 GHz) A/D channels was negligible at the low, sub 20 MHz, frequencies of interest.

Frequency response. fftlen=16384, overlap=8192, datlen=1000064, sets=1936, File:filtresp_LP1

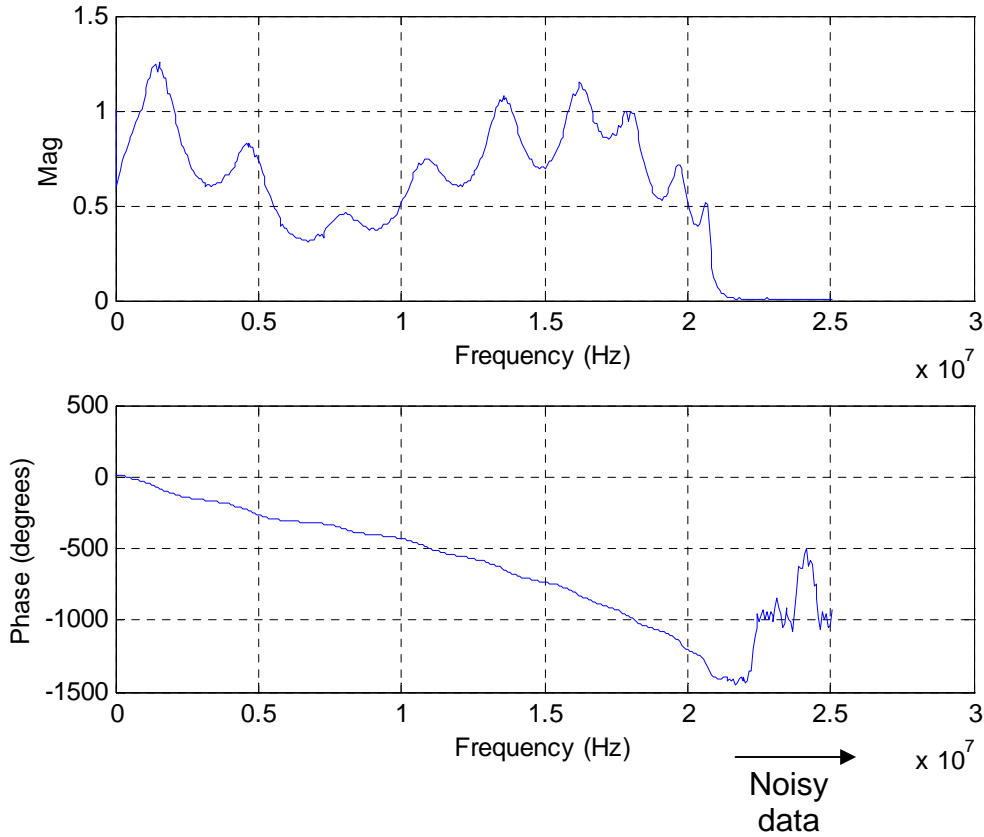


Figure 13 Frequency response for the OPM channel

The frequency dependent time delay is derived from the phase by the following expression

$$\phi = 2\pi f T_d \quad (4)$$

where ϕ is the measured phase at frequency f . The time delay is T_d . Note that the *time* delay is different from the *group* delay, which is only a measure of the slope of the phase. The time delay is the actual time it takes for a signal at a given frequency to pass through the system. The relationship between the *range* delay and the time delay is given by

$$Range_Delay = \frac{c T_d}{2} \quad (5)$$

Where c is the speed of light. The factor of two is due to the round trip path of the light in the range measurement. The derived range delay versus frequency for the pulse tone OPM is plotted in Figure 14. The ± 3.5 m of range instability is significant. Furthermore the range delay is very sensitive near 6 MHz, where the OPM is nominally centered.

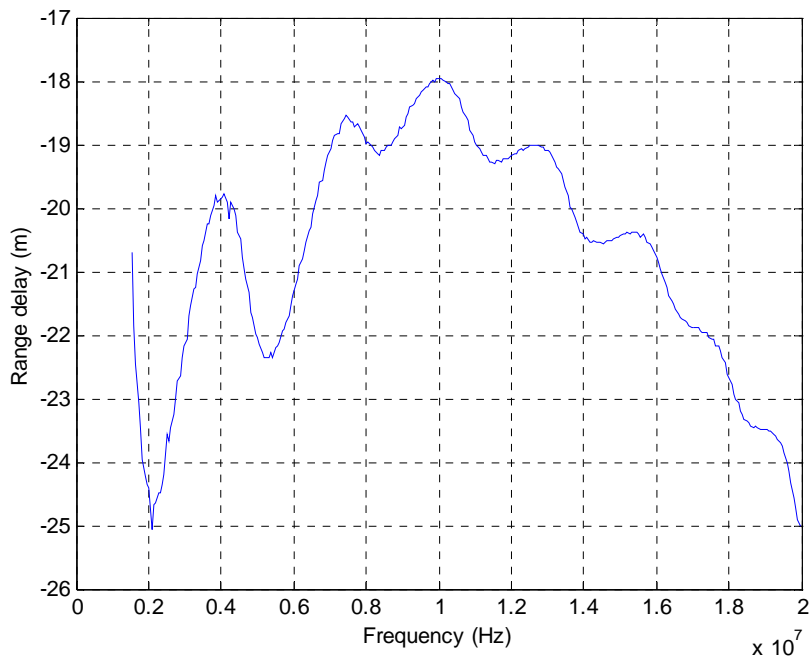


Figure 14 Range delay for the pulse tone OPM channel.

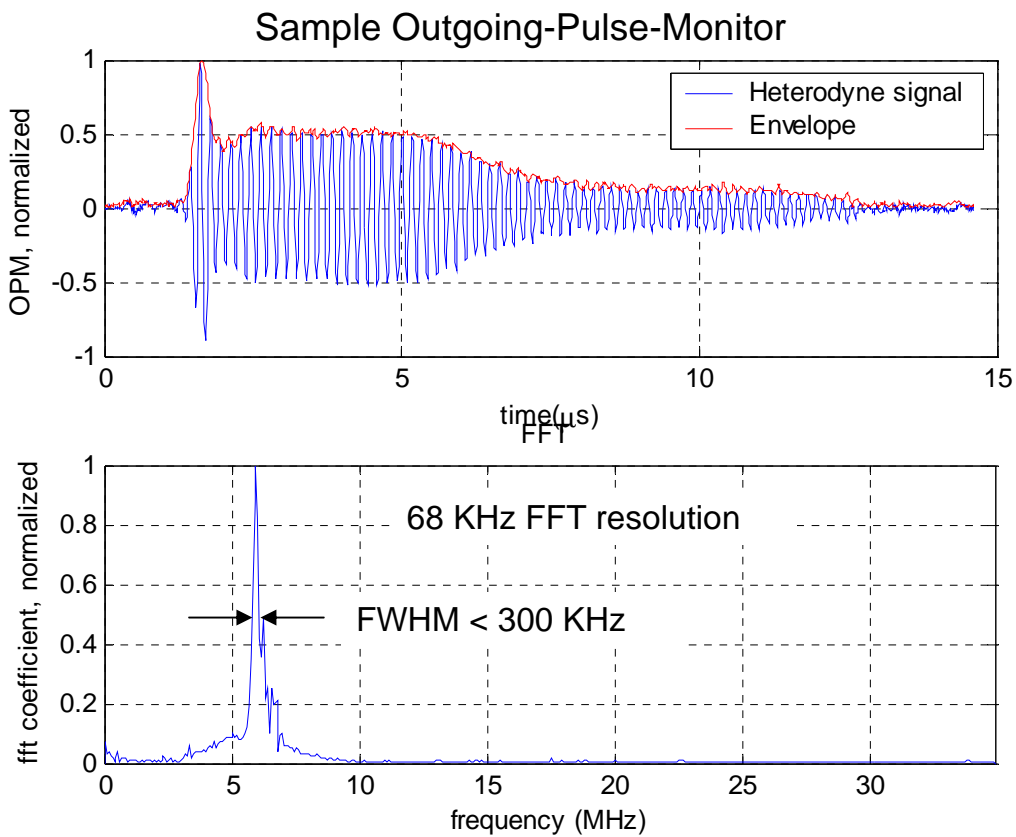


Figure 15 The top plot shows the digitized heterodyne OPM. The derived envelope is also shown. The envelope is the square root of the intensity of the direct detect signal. The lower plot shows the narrow bandwidth of the OPM of less than 300 KHz.

For a simple correction, the OPM can be assumed to be at single frequency. Figure 15 shows an example OPM and the sub-300 KHz bandwidth of the heterodyne signal. Figure 16 explores whether a simple frequency correction is possible by comparing the error of correcting using a single OPM frequency versus if the frequency is spread out uniformly over 305 KHz. The difference between the two cases is shown in the lower plot of Figure 16. The correction error is less than 0.1 m with the assumed 305 KHz box car filter if the OPM is adjusted to be greater than 5 MHz. Thus, the assumption of the OPM occurring an infinitely narrow frequency will suffice for the range correction.

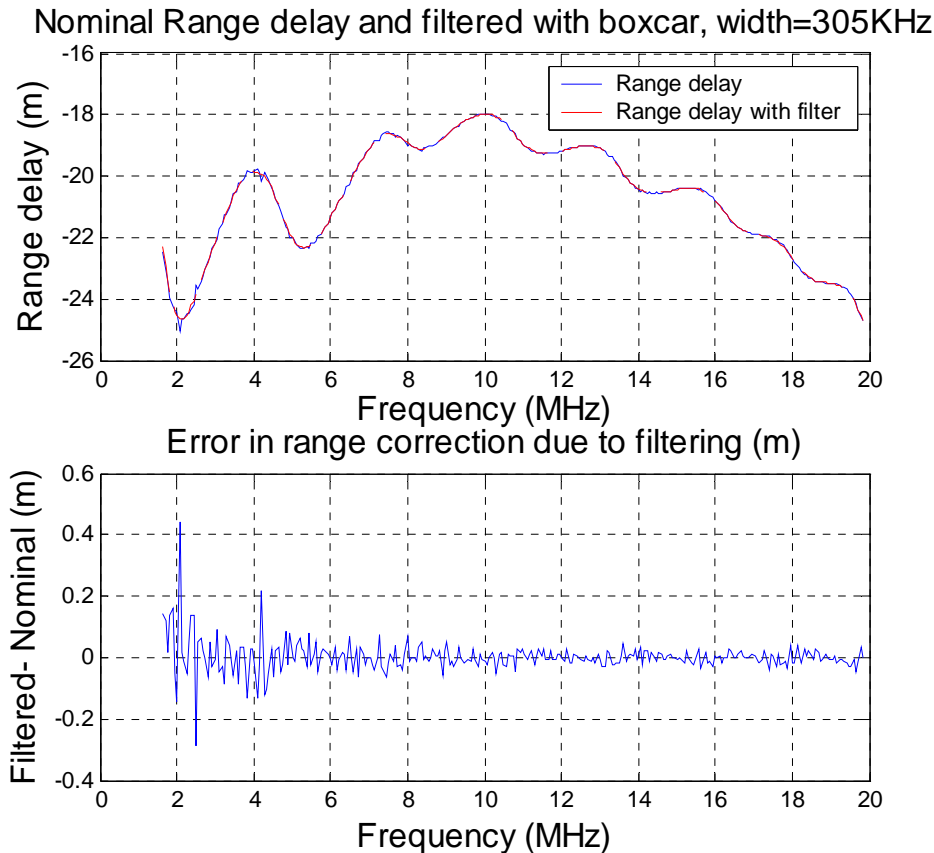


Figure 16 The top plot shows the time delay for the nominal and when the nominal is filtered with a 305 KHz wide boxcar averaging filter. The bottom plot is the difference between the two data sets. The error is small – less than 0.1 m when the OPM is controlled to be above 5 MHz.

Another source of error in the range correction arises if there is an error in the calculated OPM frequency. Figure 17 explores this error when the OPM frequency is off by a full resolution element of the FFT. Even with this extreme assumption, the range correction error is less than 23 cm when the OPM is controlled to be above 5 MHz. Thus, even after considering the bandwidth of a boxcar OPM and conservative assumptions of the frequency uncertainty, the OPM range delay correction error is small (0.25 m root sum square error). Thus, even a simple correction will produce more than an order of magnitude improvement.

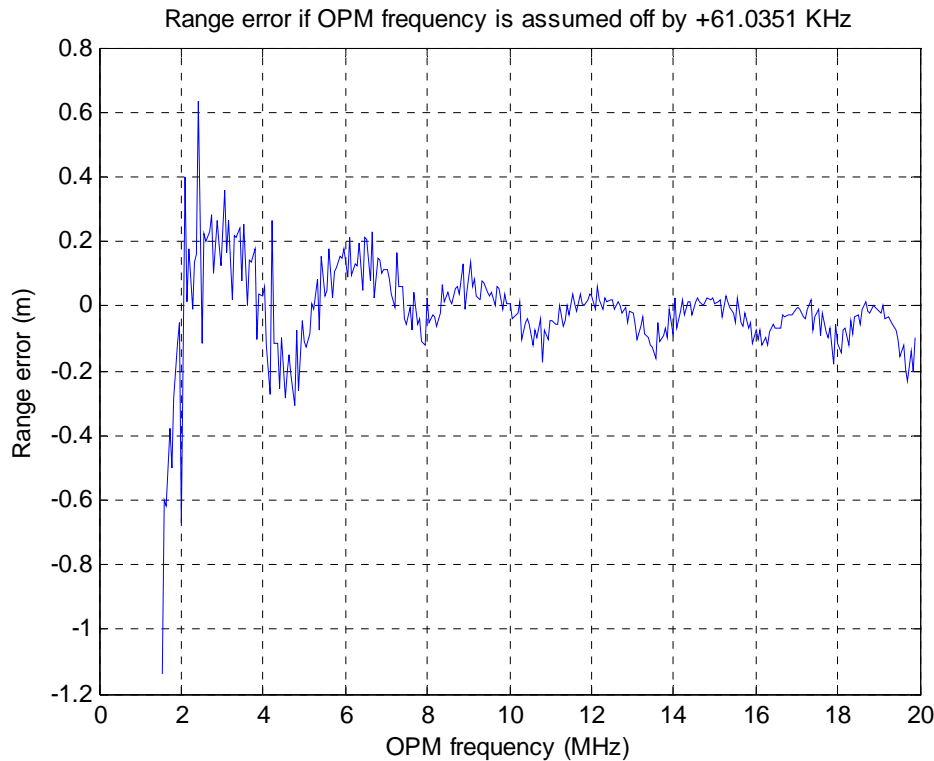


Figure 17 The range error if the OPM nominal frequency is in error by 61 KHz.

Figure 18 shows the residual after compensation for the OPM frequency. The residual is plotted versus the received frequency. The residual shows significant frequency dependence in both the in-lab and satellite data. The satellite data is from a 22195 pass on July 17, 2006. The offset of 39.3 m was subtracted from the 22195 data such that both data sets were assigned the same mean for graphing purposes. Most importantly for this current analysis, corrections of greater than ± 3 m are observed. From this data we can see that for the satellite pass and the in-lab data the received frequency can vary by more than ± 2 MHz from the mean. The variability in the received frequency for the in-lab data is essentially the same as the stability of the seed-to-local oscillator. The variability in the return frequency for the satellite is also dependent on the accuracy of the Doppler frequency tracking. The tracking of the Doppler shift is typically on the order of ± 2 MHz from the mean for the several Lageos satellite passes that were examined during this study. However, the mean received frequency for a satellite can be off by more than 10 MHz. The HI-CLASS system does have the capability for the operator to control an offset to the VFO frequency, which would control the mean return frequency better. Other Doppler tracking features that feedback the measured Doppler shift may be considered in future work. Because the laser return data has a significant standard deviation and errors of interest are sub-meter, large numbers of returns would be required to get a high resolution frequency response for the receiver. A similar all electrical test as the OPM is highly desirable. The receiver test would need to use digitizers with more than 2 GHz sampling. This test, along with corrections for the A/D board frequency responses is an area for future work. The work in this paper, highlights that the non-

constant time delays in the heterodyne receiver are significant and justifies the further tests. Future work will seek to implement high resolution frequency responses considering the receiver, A/D boards, and VFO tracking. Furthermore, hardware upgrades may be implemented that reduce the frequency sensitivity of the system.

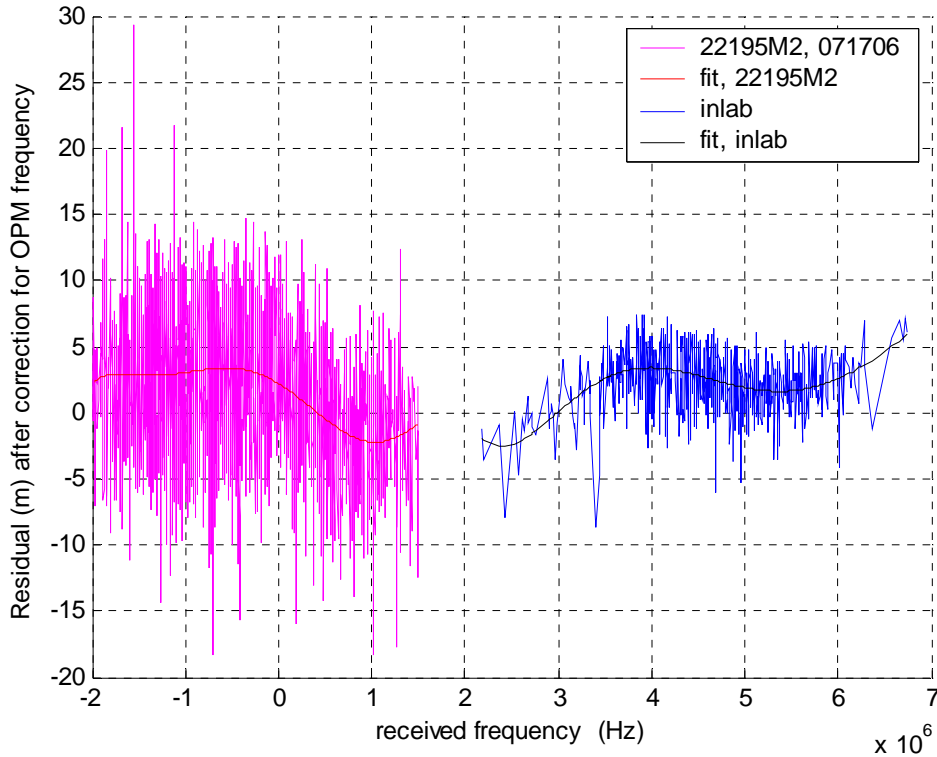


Figure 18 The residual after the OPM frequency correction plotted versus the received frequency. The in-lab data is the set centered around 4 MHz. The Lageos-II (Obj #22195) data set is centered near 0 MHz. The fit shows the residual is dependent on the received frequency.

5. Velocity Metrics

Velocity metrics from HI-CLASS have typical standard deviations of 0.25 m/s to 0.5 m/s off from the Lageos satellites. This stability is limited by the stability of the local oscillator over the time of flight.

Figure 19 shows the drift of the local oscillator as it was referenced to an MIT Lincoln Laboratory “ultra-stable” laser. The “ultra-stable” laser is believed to have a frequency stability better than 10 Hz in a 100 ms observation time⁷. The corresponding error in

⁷ I. Melngailis, W. E. Keicher, C. Freed, S. Marcus, B. E. Edwards, A. Sanchez, T. Y. Fan, and David L. Spears, “Laser Radar Component Technology”, Proceedings of the IEEE, Vol 84, No 2, February, 1996.

velocity when it is used as a local oscillator reference is 60 microns per second, which is negligible for our purposes.

The observed drift of the HI-CLASS local oscillator for this particular data set is a monotonic drift of about 140 KHz in 100 ms with high frequency variations of ± 50 KHz. As an example, for an object at 6 Mm (40 ms time of flight) this frequency instability corresponds to a velocity error of 0.3 m/s with an additional 0.3 m/s due to the high frequency component.

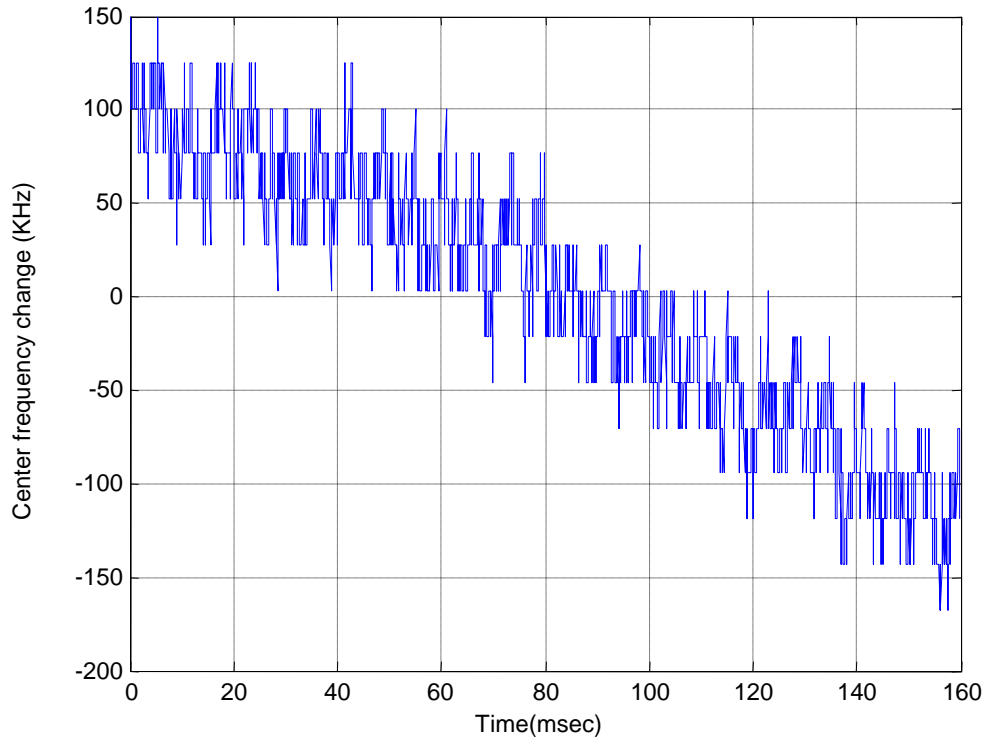


Figure 19 The spectrograph of the LO-stable laser beat versus time. The vertical axis is the center frequency change from the average beat frequency of 8.6 MHz. The frequency resolution of the FFT used to generate the spectrograph is 24 KHz.

The velocity stability in-lab, where the time-of-flight is essentially zero, is much better than observed from satellites as seen in Figure 20. The top plot is the CNR for in-lab ranging data. The CNR was adjusted by adding noise, which resulted in a 28 dB average. The lower plot is the resulting raw in-lab velocity. The 4 cm/s velocity sigma is much better than the best 25 cm/s stability that has been observed on satellites. This raw data needs to be corrected for the -.2 m/s offset, which can also be controlled with the VFO setting. The observed velocity precision is consistent with the Cramer-Rao bounds where

$$\sigma_v = \frac{\lambda}{2T\sqrt{CNR}} \quad (6)$$

Here σ_v is the rms velocity precision. The variable T is the laser pulse length and can be assumed to be on the order of 6 microsec. At 28 dB CNR, the velocity precision that is

expected is about 4 cm/s. In the high CNR limit, the noise floor of the in-house ranging is 2 cm/s. This noise floor is attributed to frequency instability within the receiver. More importantly, the 2 cm/s noise floor is much better performance than HI-CLASS has achieved off satellites where the local oscillator stability dominates.

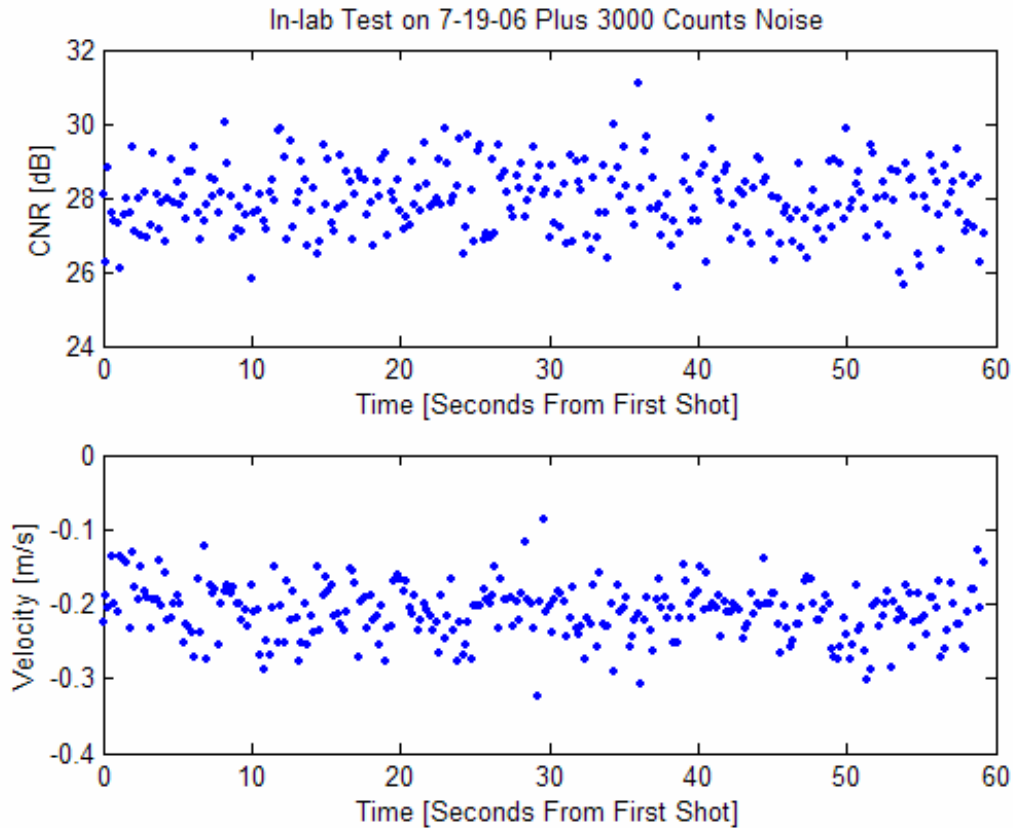


Figure 20 The top plot is the CNR for in-lab ranging data. The CNR was adjusted by adding noise such that it was about 28 dB. The lower plot is the resulting raw in-lab velocity.

Figure 21 shows the velocity residual for a segment of a Lageos II pass. The velocity correction derived from the LO-stable laser beat is also shown. The LO-stable laser drift correction accounts for most of the residual. After correction for the LO instability, the residual is 17 cm/s rms. Even though this performance is worse than the two cm/s noise floor that has been demonstrated in-lab, it is the best achieved velocity performance to date for the HI-CLASS system to a satellite at Lageos distances. It is believed that the performance can reach the in-lab noise floor level after more precisely synchronizing the TEA laser signals and the LO-stable laser beat signals on the two separate data acquisition systems. Similarly, the high frequency variations of the local oscillator necessitate exquisite timing and signal processing.

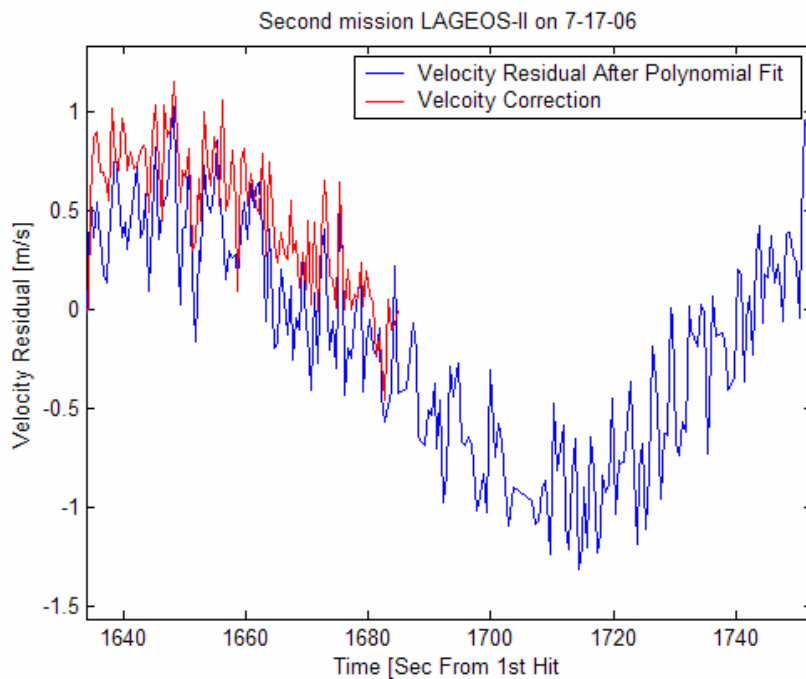


Figure 21 The velocity residual versus time for a Lageos II pass. The velocity correction derived from the LO-stable laser beat is also shown. The velocity residual from the satellite is largely attributable to the local oscillator stability.

6. Conclusions

Highly accurate ILRS-based “truth orbits” were used to assess the ranging accuracy of the HI-CLASS system. Through this method, a ± 2 m “bias” instability was successfully identified.

Errors due to timing errors and time delays were investigated. A timing technique was developed to measure system timing errors over the full time-of-flight. A sub-ppb time-base accuracy was demonstrated and a timing noise jitter of 5 cm (0.3 ns) is reported. Having ruled out the timing system errors, the time delay can now account for the significant remaining range instability. The frequency response of the OPM, which was measured with high resolution, can account for ± 3.5 m of range instability. Furthermore, the frequency response of receiver can account for ± 3.0 m of range instability. These errors are worst case since the limited frequency spread and averaging over the pass reduces the possible bias. Based on the OPM frequency response, a look up table correction technique can be readily applied with an accuracy of about 0.25 m.

The limiting velocity error source was also investigated. The stability of the local oscillator limits the velocity accuracy. Velocity corrections using the local

oscillator/stable laser beat have enabled the best HI-CLASS Doppler residual so far under relatively unstable local oscillator conditions.

Acknowledgements

This work was supported under contract FA9451-04-D-0056 to AFRL.